Molecular Dynamics Simulation Study of Transverse and Longitudinal Ionic Currents in Solid-State Nanopore DNA Sequencing

Mohsen Farshad and Jayendran C. Rasaiah*

Cite This: https://dx.doi.org/10.1021/acsanm.9b02280

Read Online

| ACCESS | Metrics & More | Article Recommendations | SI Supporting Information |

ABSTRACT: We report all-atom molecular dynamics (MD) simulations of single-stranded DNA (ssDNA) translocation in 1 M KCl solution through a silicon nitride solid-state nanopore with one or two nanochannels perpendicular to the nanopore. We measure the longitudinal and transverse ionic currents generated through the pores under voltage biases applied longitudinally and transversely across the pores. During fast translocation of homo-oligonucleotides through the pore, the characteristic signals of nucleotides resulting from ion—nucleotide interactions cannot be distinguished. These signals are buried in fluctuations of the ions caused by thermal energy at high sampling frequency. A pattern recognition neural network shows that the averaged transverse and longitudinal ionic currents and their combination enable the canonical A, G, T, and C nucleotide classifications to be recognized with an accuracy of 81.4%. Further improvements can be explored with machine learning algorithms, larger databases, and slower translocation rates at lower voltages biases that would require greater computer resources.

KEYWORDS: solid-state nanopore, DNA sequencing, nanochannel, ionic current, molecular dynamics

Ionic currents in three directions → Ion-nucleotide interactions with three orientations
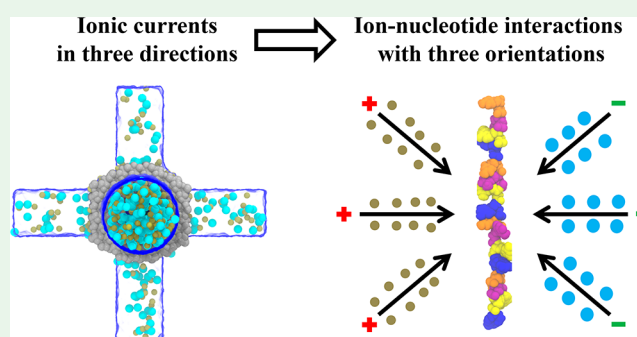
INTRODUCTION

Nucleotide-dependent stepwise modulation of the ionic current during voltage-driven translocation of single-stranded DNA (ssDNA) through a narrow nanopore is the basis of nanopore DNA sequencing. The idea of using nanopores for single molecule detection emerged over three decades ago.[1,2] Negatively charged polynucleotides traverse in the direction of an electric field through a nanopore of suitable diameter.[2,3] Kasianowicz stabilized an α-hemolysin nanopore embedded in a lipid bilayer membrane for several hours using a 1 M KCl solution.[3] In 1996, Kasianowicz et al. suggested characterizing individual polynucleotide macromolecules by translocating them through α-hemolysin under an applied electric field.[3] Seven α-hemolysin monomer amino acids secreted by *Staphylococcus aureus* bacteria self-assemble into a lipid bilayer membrane to create a biological α-hemolysin nanopore with a diameter varying from 2 to 1.4 nm at its narrowest point and a constriction commensurate in size to the diameter of a single-stranded polynucleotide.[4] It was found that the duration of ionic current blockage corresponds to the residence time of different lengths of polynucleotide sequences.[3,5−7] The same group was able to discriminate between homopolymer polynucleotides by measuring the modulation of ionic current across the membrane.[8] Later, Meller et al. found that different polynucleotide sequences generate distinguishable transloca-tion time patterns in ionic current blockade scatter plots.[9,10]

To date, researchers have used ionic currents,[8−11] transverse tunneling currents,[12,13] capacitance measurements,[14−16] fluo-rescent readout,[17] and photon counting[18,19] for detecting polynucleotides. These studies opened new possibilities in single molecule detection, which could potentially result in more efficient and less costly techniques for sequencing DNA.[20−23]

Other biological nanopores that have been tested in nanopore sequencing methods include *Mycobacterium smegmatis* porin A (MspA) and Curlin sigma S-dependent growth subunit G (CsgG).[24−29] The MspA nanopore has a diameter of 1 nm at its constriction.[24] The engineered MspA mutant nanopore has been shown to improve the translocation of polynucleotides for the purpose of single polynucleotide detection.[24−27] In addition, an engineered derivative of the CsgG nanopore used by Oxford Nanopore Technology shows high accuracy detection and long-read sequencing of polynucleotides.[22,28,29] Biological nanopores have many advantages including dimension reproducibility as a result of compatibility with chemical modification processes and a low

rate of translocation through nanopores, which increases the time for ion-nucleotide interactions and detection.[30,31] However, protein nanopores are highly dependent on the conditions of the system, and the lipid bilayer that supports the nanopore is not stable.[30,31] Extensive achievements in DNA sequencing are gained by using biological nanopores.[32]

Synthetic nanopores, which are termed solid-state nanopores, are an alternative to biological nanopores and have been utilized in nanopore sequencing studies.[31,33−35] Solid-state nanopores are more robust and stable in a variety of conditions than biological nanopores[31,33−35] and can be manufactured with different sizes and shapes.[36−39] In addition, they can be integrated into electronic and optical devices.[40,41] These advantages make solid-state nanopores suitable candidates for future nanopore DNA sequencing technology. In 2001, Li et al. developed an ion-beam sculpting method for fabricating 1.8 nm nanopores with the aim of single molecule DNA detection.[42] Currently, nanopore fabrication is primarily achieved using electron-beam lithography.[36,43] Li et al. reported the first use of a solid-state nanopore to detect double-stranded DNA (dsDNA).[42,43]

Early molecular dynamics (MD) simulations of the voltage-driven translocation of biomolecules through nanopores provided atomic resolution of the phenomenon.[44−46] The simulations provided insight into the translocation of ions and biomolecules through solid-state and biological nanopores.[44−46] In addition, MD simulations have been performed for systems with Si_3N_4 nanopores for the translocation of ssDNA, with one or more nanochannel perpendicular to the pore to measure the transverse ionic currents with respect to ssDNA and proteins.[47,48]

In this work, we have developed a silicon nitride (Si_3N_4) model containing a perpendicular nanopore and nanochannels. Following previous MD studies on nanopore DNA sequencing, we solvated the Si_3N_4 and ssDNA in an aqueous solution of 1 M KCl, as described in the Computational Methods section. Using the simulations, we studied the translocation of straight oligonucleotide ssDNA through the nanopore under a longitudinally applied electric field in the presence of a transversely applied electric field across the pore. In addition, we investigated the transverse and longitudinal ionic current during the translocation of oligonucleotides through the nanopore and classified the currents of homo-oligonucleotides A, G, T, and C using neural network (NN) machine learning.

We wanted to enhance the detection of nucleotides by combining transverse (axial) and longitudinal (radial) ionic currents. As longitudinal ionic current interactions with nucleotide provide information for nucleotide detection, we assumed transverse ionic current interactions with nucleotide also provide information for sequencing ssDNA. We speculated that using two or more transverse ionic currents would provide more information than a single transverse ionic current in combination with longitudinal ionic currents by using pattern recognition NN.

■ COMPUTATIONAL METHODS

Molecular Dynamics (MD) Simulations. The 3D-DART Web site was used to create dsDNA $(AGTC)_4$, poly$(A)_{16}$, poly$(G)_{16}$, poly$(T)_{16}$, and poly$(C)_{16}$ sequences.[49] VMD was used to prepare and visualize the systems for simulations.[50] The silicon nitride nanosheet was solvated in cubic water reservoirs, and K^+ and $Cl^−$ ions were distributed in the reservoirs to give a concentration of 1 M while maintaining the

density of water, 1 g/mL. To achieve a cost-effective system in terms of computer simulation time and processor usage, we modified the cubic system to the system presented in Figure 1a as a general scheme of our model to reduce the size of the systems. The all-atom MD simulations were performed on a University of Maine supercomputer using the NAMD2 program.[51] The CHARMM27[52] was used to implement the interaction between atoms including the TIP3P model for water and CHARMM-compatible parameters[37] for silicon nitride nanosheet in the systems. We used boundary forces and periodic boundary conditions implemented in NAMD2 on the edges of the reservoirs to preserve the nanocubic and cylindrical shapes of the systems in the simulations. After minimization of the systems, we equilibrated them in an NVT ensemble. The temperature was 300 K, and the volume and number of atoms varied between systems, but the number was over 100000 atoms after modification. The Verlet algorithm implemented in NAMD2 was used to integrate the equations of motion to compute the time evolution of the atom position and velocity trajectory every 2 fs time step. The atom position frames were recorded every 1 ps (each 500 time step) for later analysis. A cutoff distance of 12 Å was defined for short-range electrostatic and van der Waals interaction. Particle mesh Ewald (PME)[53] was used to implement long-range electrostatic interactions in the system with a grid spacing of 1 Å. The short dsDNA oligonucleotides were converted to two ssDNA sequences. Then, the applied electric fields implemented in NAMD2 straightened the ssDNA without the contribution of the solvent, solute, or nanosheet by fixation of the oxygen of the hydroxyl group on the backbone of the ssDNA at one end. Introduction of the electric field in our simulations generated the ionic currents and drove the ssDNA through the Si_3N_4 nanopore. The movement of ssDNA atoms was harmonically restrained in the x and y directions. This means the ssDNA atoms can only oscillate around their center of mass in x and y directions while they are free in the z direction. All the atoms in silicon nitride nanosheet are fixed in their positions.

Electric Ionic Current. Following equation was used to calculate the electric field using trajectories of the MD simulations:

$$I(t) = \frac{1}{l_a \Delta t} \sum_{i=1}^{N} q_i [a_i(t + \Delta t) - a_i(t)] \qquad (1)$$

In eq 1, the q_i is the charge of atom i which is −1 or +1 for $Cl^−$ and K^+, respectively. Δa_i is the distance that the ith ion is traversed in the direction of a, which is a general notation for the x-, y-, or z-axis. l_a is the nanosheet length in the direction of a. Δt is the time step of our simulations, which is 1 ps.

Moving Average Filter. A simple moving average filter smoothed out the noisy electrical signals calculated from time series trajectories obtained from the MD simulations. We employed the movemean function in MATLAB that consecutively calculates the arithmetic average of a given subset of length k in data and a sliding window of the same length through the time series data. The movemean function creates an output of smooth electrical signals with the same length of the original signals. We used a moving average filter with a window of 5 ns for calculation of error bars in transverse and longitudinal bar graphs as well as in 2D and 3D scatter plots and a window of 1 ns for cross-correlation calculation.
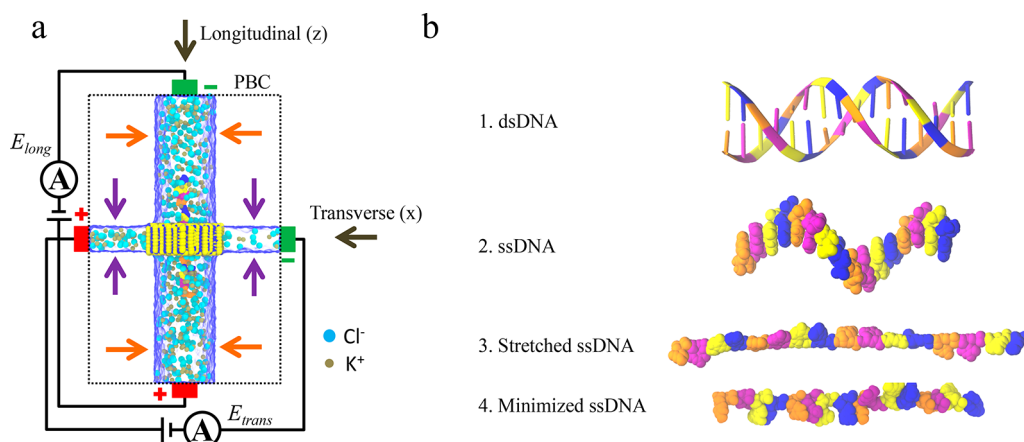
Figure 1. MD simulation of nanopore DNA sequencing by measuring ionic currents generated under longitudinal and transverse electric fields during translocation of minimized oligonucleotide ssDNA. (a) General schematic representation of the model including both transverse and longitudinal electric fields. The blue continuum represents water; the 1.8 Å diameter cyan and 1.3 Å diameter brown spheres represent Cl^- and K^+ ions in water, respectively. The vertical yellow-blue cylinder in the center is the Si_3N_4 nanopore. The Si_3N_4, Cl^- and K^+ ions, and ssDNA with a sequence of $(AGTC)_4$ are shown with van der Waals (vdW) sphere representations. Transverse and longitudinal electric fields, E_{trans} and E_{long}, respectively, were applied in the system. Purple and orange arrows respectively are the examples of the directions of applied spherical and rectangular forces used in the model to preserve the integrity of the reservoirs. The dotted rectangle shows the periodic boundary condition (PBC). (b) Step-by-step transition from dsDNA (b1) to minimized straight oligonucleotide ssDNA (b4).

Cross-Correlation. The cross-correlation of the x and y discrete-time series as a function of the lag m is defined by following discrete equation:

$$\hat{R}_{x,y}(m) = \sum_{n=0}^{N-m-1} x_{n+m} y_n^*$$

(2)

where x and y^* (complex conjugate of y) are vectors with a length of N. Before cross-correlation calculation of the transverse and longitudinal ionic currents, the noise in signals was smoothed out by using moving average filter over a window of 1 ns. The output length of cross-correlation sequence is $2N - 1$.

Neural Network. We employed a pattern recognition neural network (NN) which is a feed-forward neural network to classify the target classes using MATLAB. We used two layer neural networks with one hidden layer and 248 neurons. The Levenberg−Marquardt (LM) transfer function was used to train the data. The mean-square error (MSE) functions were used to calculate prediction error of results from labeled classes.

RESULTS AND DISCUSSION

We studied three different systems using MD simulation.

System 1: Voltage Dependence of ssDNA Stepwise Translocation and Ionic Currents for the $(AGTC)_4$ Sequence. Following extensive work performed by other groups, we performed all-atom molecular dynamics (MD) simulations on three different systems.[14−16,44−48] Figure 1a shows a schematic of our model in which we measured transverse and longitudinal ionic currents generated under transversely and longitudinally applied electric fields. The ionic currents were analyzed during the translocation of straight oligonucleotide ssDNA as they potentially carry distinct information for the four nucleotide types. If the number of nucleotides decreases along the path of the ionic current in the pore, the classification of signals into four nucleotide categories becomes more probable. For these reasons, we used a narrow nanopore and linear ssDNA rather than dsDNA to reduce the

complexity of the problem.[54,55] Figure 1b schematically shows the steps in converting dsDNA to straight ssDNA (described in the Computational Methods section). In this model (systems 1−3), nitrogen atoms charges are set to −0.575925 and silicon atoms charges are set to +0.7679. The total charge of Si_3N_4 is approximately set to zero (e.g., total charge in system 2 is $\sim-1.79 \times 10^{-7}$). There are negative (N) and positive (Si) atoms on the surface of the Si_3N_4 nanosheet that can be effective along with K^+ and Cl^- ions in facilitation of electro-osmotic flow.

We used MD simulations of system 1 (Figure 2) to evaluate the rate of oligonucleotide ssDNA—$(AGTC)_4$—translocation through the Si_3N_4 nanopore with three different longitudinal voltage biases (0.5, 1, and 2 V) in the longitudinal direction along the pore. Furthermore, we wanted to know whether a transverse electric field with high voltage bias eliminates stepwise translocation of oligonucleotide through the nanopore. In this regard, these simulations were performed in the presence of a transversely applied voltages of 4 V across the reservoir and Si_3N_4 nanochannel. Water electrolyzes at voltages higher than 1.2 V. However, the force fields and models in our MD simulations would not account for the electrolysis of water. Larger voltages enabled us to more easily explore trends in shorter computer time that provide information about lower voltages assuming the effects are approximately linear. A direct MD study of nucleotide translocation in pores at low voltages would slow translocation rates and enhance nucleotide discrimination but would require much greater computing resources than are available for this study.

In this model, the Si_3N_4 nanopore with thickness of 2.4 nm contains an elliptical longitudinal nanopore with an average diameter of 2.4 nm and an elliptical transverse nanochannel with a diameter of 1.8 nm. Figure 2a,b demonstrate two graphical perspectives of system 1 in which oligonucleotide ssDNA is translocating through a Si_3N_4 nanopore in a longitudinal direction. The transverse nanochannel and longitudinal nanopore, along with the oligonucleotide ssDNA, were immersed in a solution of 1 M KCl. The periodic boundary condition (PBC) employed in these
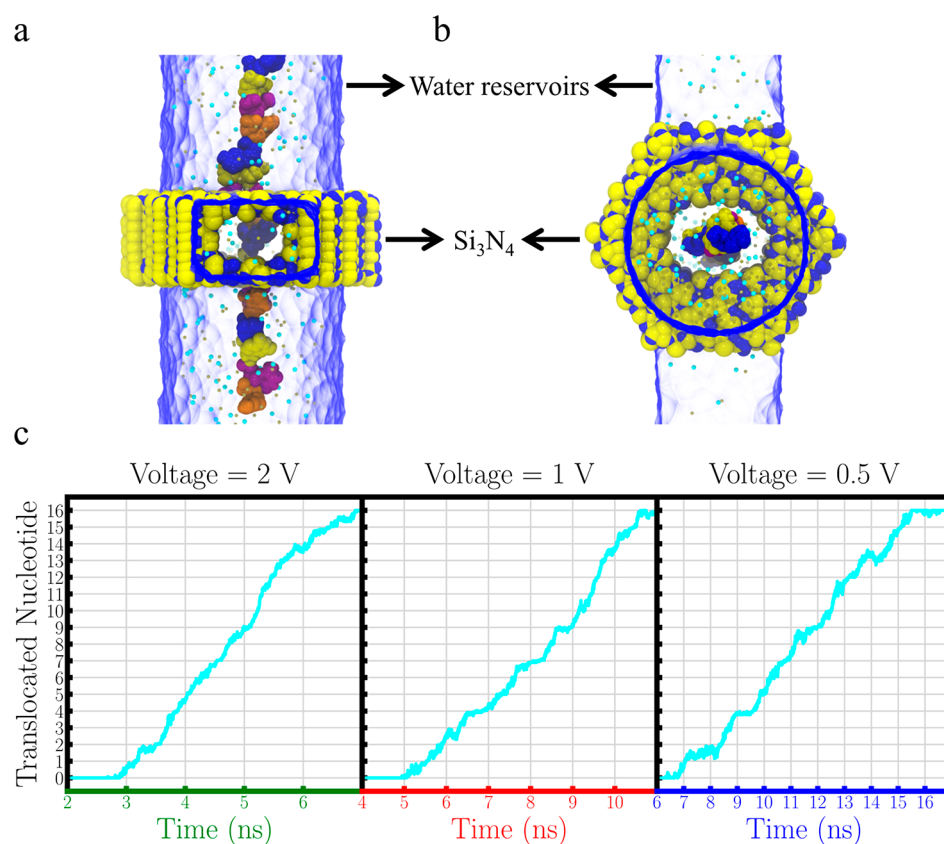
Figure 2. System 1: translocation behavior of oligonucleotide ssDNA through a Si_3N_4 nanopore. (a, b) Two perspectives of system 1 along the x- and z-axes through transverse nanochannel and longitudinal reservoirs, respectively. The blue continuum represents water; the large cyan and small brown scale van der Waals (vdW) representations are Cl^- and K^+ in water, respectively. The Si_3N_4 and $(AGTC)_4$ ssDNA sequence is shown with vdW representation. (c) Number of nucleotides translocated through the longitudinal nanopore as a function of time (ns).

simulations was a cubic box that does not apply on other edges of the reservoirs. In addition to the PBC, we used boundary forces to create virtual walls around the edges of the reservoirs that are away from the PBC. Figures 2a and 2b are the top and side views of the system, respectively, illustrating the two shapes of the reservoirs. The shape of the reservoirs was determined by the force introduced in the simulations. We have defined confining forces to maintain the integrity of the water and ions in the reservoirs and prevent them from dispersing into the empty region defined by the PBC. To keep the ssDNA straight, we limited the translocation of the oligonucleotide to the longitudinal direction by harmonically restraining the movement of backbone atoms in the x and y directions. Nucleotides in a straight oligonucleotide translocate through the nanopore consecutively in a longitudinal direction under an applied electric field. Consequently, the interference of neighboring nucleotides in the ionic current modulation for each individual nucleotide is minimized, which may improve the distinguishability of the signals for the four types of nucleotide. The Si_3N_4 atoms are fixed in their positions to avoid a significant change in the shape and position of the nanosheet in the system.

For system 1, we performed five sets of simulations for each voltage bias to obtain a relatively large number of signals for statistical analysis. We calculated the translocation rate (nt/ns) of $(AGTC)_4$ ssDNA under applied voltages of 0.5, 1, and 2 V (Figure 2).

Figure 2c shows that the presence of a transverse electric field of 4 V does not affect or eliminate the stepwise

translocation of ssDNA through nanopores.[54,56−58] The small DNA−nanopore friction forces in solid-state nanopores compared with in biological nanopores lead to fast DNA translocation.[55,59,60] DNA−nanopore interaction is among the factors that control the rate of DNA translocation through a nanopore.[59−62] Fast translocation of oligonucleotide ssDNA through a nanopore under applied voltage bias therefore implies low interaction forces between the harmonically restrained (in the x and y directions) oligonucleotide and the Si_3N_4 nanopore during translocation through the middle of the nanopore. In addition, restraining the ssDNA in the x and y directions inside the water reservoirs restricts the entropy as a result of there being a limited number of available conformations. Therefore, we assume that the entropy of the ssDNA does not decrease significantly when it translocates through the middle of the nanopore.

We performed five independent simulations for each 0.5, 1, and 2 V voltage biases. The average of translocation rate (nt/ns) for each voltage is shown in Figure 3a. When the voltage increases, the electromagnetic force on oligonucleotide DNA with 15 negative charges of phosphate groups increases and leads to faster translocation of oligonucleotide DNA. Figure 3a shows that the nucleotide (nt) translocation rate in this system is around 1 nt/ns under 0.5 V applied voltage bias. This is considered fast in comparison to actual experiments for nucleotide detection.[63,64] In experiments, the detection speed is governed by the redox reaction between electrode such as silver/silver chloride electrode and ions in solution at the electrode interface. Advanced amplifiers record signals with a
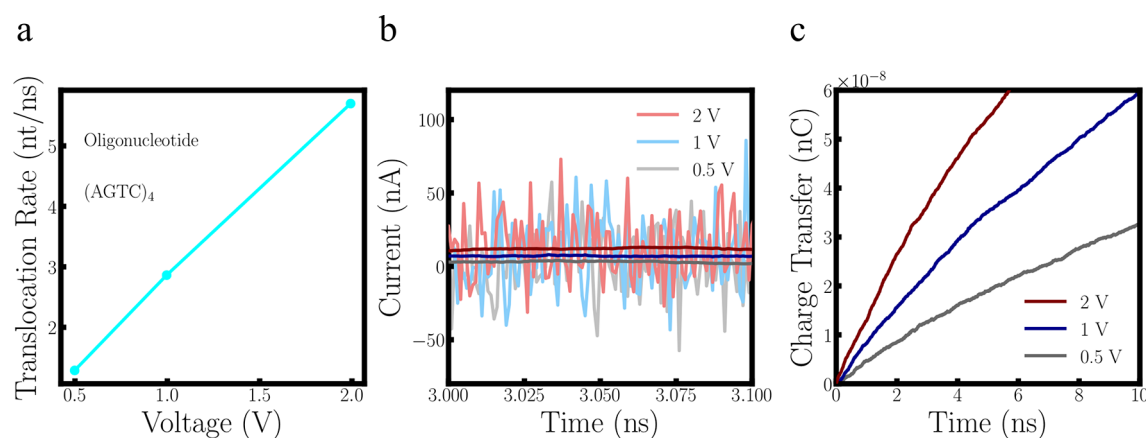
Figure 3. System 1: Analysis of current and translocation rate. (a) Average translocation rate (nt/ns) of oligonucleotide ssDNA, $(AGTC)_4$, under three voltage biases: 0.5, 1, and 2 V. (b) 100 ps time lapse of the instantaneous longitudinal current during translocation of oligonucleotide ssDNA, $(AGTC)_4$, through the longitudinal nanopore under three applied voltage biases: 0.5, 1, and 2 V. (c) Charge transfer through the longitudinal nanopore during oligonucleotide translocation as a function of time for three voltage biases: 0.5, 1, and 2 V.

bandwidth of 1 MHz, which is compatible with the ionic current production mechanism.[65,66] In our simulations, the ionic current is governed by small ion displacements across the pore in each time frame with sampling frequency of 1 THz (described in the Computational Methods section). As a result, with a translocation rate of around 1 nt/ns under an applied voltage bias of 0.5 V, we obtain 1000 signals per nucleotide, which may provide adequate information for classification.

Figure 3b shows a 100 ps time lapse of the longitudinal ionic current signals under three different applied voltage biases during the translocation of oligonucleotide ssDNA through Si_3N_4 nanopores. As described in the Computational Methods section, the ionic current signals are generated by the K^+ and Cl^- ion displacements in the nanopore and nanochannel under applied electric fields along and across the system. As the current signals were noisy, we smoothed them by taking averages within a sliding window of 200 ps in length. The averaged data are shown in high-intensity colors in Figure 3b. The smoothed lines demonstrate a voltage dependence trend for the instantaneous longitudinal ionic currents generated by voltage-driven ions. The cumulative ionic currents over time confirm a relative increase in current with increasing voltage (Figure 3c).

System 1 demonstrated the stepwise translocation of oligonucleotide ssDNA through a Si_3N_4 nanopore in the presence of a transverse electric field. We also confirmed that the translocation rate of oligonucleotides depends linearly on the applied voltage.[3,10,62] Furthermore, the longitudinal ionic current was directly proportional to the applied voltages.[44,67] This system provides insight into the randomness of noisy signals with high frequency fluctuations. We used a moving average filter to smooth the ionic current signals as described in the Computational Methods section. We were then able to distinguish the correlation between the oligonucleotide translocation rate through the nanopore and the longitudinal ionic current, with electric field, and studied two additional systems to distinguish between different homo-oligonucleotides. In these simulations, all the oligonucleotides contain 16 nucleotides including 15 negatively charged phosphate groups with K^+ ions from 1 M KCl aqueous solution as the counterions.

The same principle for boundary forces and restraints was applied to systems 2 and 3, as described below and in the Supporting Information. The magnitude of the electric field, thickness of the nanosheets, and the size of the nanopores and nanochannels are the key variables that were addressed. In both systems we studied the average translocation time (ns/nt), the averaged ionic currents (nA) along both the longitudinal and transverse directions, the Kernel probability distribution of instantaneous ionic currents, the combination of longitudinal and transverse electric signals using scatter plots, and the cross-correlation between them.

System 2: Two Transverse Currents and One Longitudinal Ionic Current through a Si_3N_4 Nanosheet. We created system 2 to investigate the combination of two transversely and one longitudinally filtered signals. We also designed system 3 with one transverse and one longitudinal Si_3N_4 pore as described in the Supporting Information. Realization of a narrow nanochannel through an ultrathin silicon nitride nanosheet may not seem practical. However, with fast growing nanomaterial fabrication technology realization of this model is in principle achievable. System 3 has a precisely designed narrow nanopore to accommodate fewer nucleotides than systems 1 and 2, while still having a nanochannel that allows the passage of ions to generate an ionic current under a transversely applied electric field. We used higher transverse voltages of 4 and 10 V for system 3 in comparison to transverse voltages of 0.5 V for system 2 because the diameter of transverse nanochannel in system 3 (0.8 nm) is significantly smaller than the diameter of transverse nanochannel in system 2 (1.4 nm). We speculated that a higher electric field for narrower nanochannel is required to push adequate number of ions through the narrow transverse nanochannel for interaction with nucleotides in the nanopore region. The detailed results for system 3 are presented in the Supporting Information. Figure 4a is a perspective of the system 2 through the x-axis displaying two transverse reservoirs and one longitudinal reservoir. Figures 4b and 4c show two orientations of nucleotides recorded simultaneously through two transverse nanochannels in the x and y directions. We are therefore measuring the ion−nucleotide interactions with three orientations of nucleotides including the longitudinal nanopore. The thickness of the Si_3N_4 sheet is 2.4 nm with cylindrical transverse nanochannels and cylindrical longitudinal nanopore diameters of 1.4 and 2 nm, respectively. Figure 4d is a top view representation of the system along the z-axis.
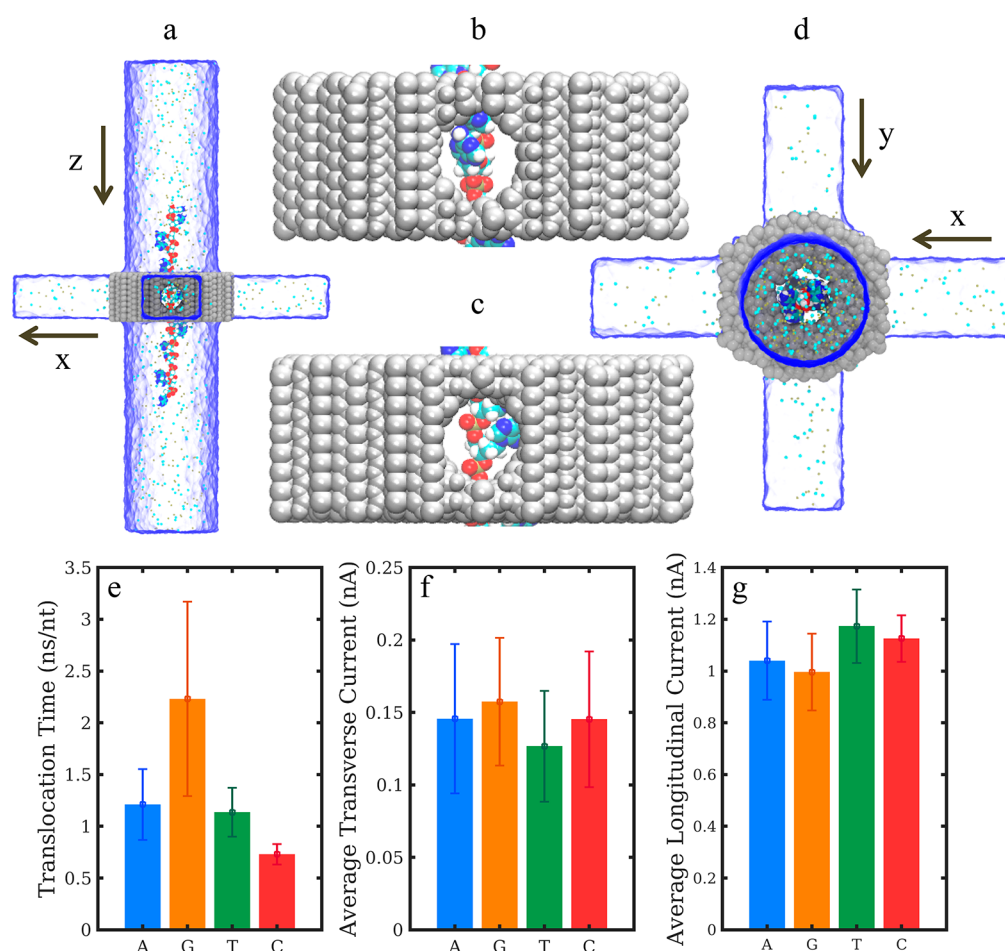
Figure 4. System 2: translocation of four types of homo-oligonucleotide through a longitudinal Si$_3$N$_4$ nanopore and calculation of two transverse currents and one longitudinal ionic current. (a) A perspective of system 3 from the y direction. The blue continuum represents water reservoirs passing through the Si$_3$N$_4$ nanopore and two nanochannels in the Si$_3$N$_4$ nanosheet—represented by the gray areas—during translocation of adenine homo-oligonucleotide ssDNA, (A)$_{16}$. The large cyan and small brown spheres are the vdW representations of Cl$^-$ and K$^+$, respectively. (b, c) Two perspectives from the x and y directions in the same time frame showing two different nucleotide orientations inside the nanopore. (d) A perspective from the z direction. The colors in (d) represent the same species as (a). (e) Average translocation time (ns/nt) of each homo-oligonucleotide. (f, g) Average transverse and longitudinal ionic currents (nA) for four types of homo-oligonucleotide.

In system 2 we applied 0.5 V voltage biases along the x-, y-, and z-axes across the transverse nanochannels and longitudinal nanopores. We performed five sets of simulations for each homo-oligonucleotide type: A, G, T, and C. The transverse ionic currents along the x- and y-axes and longitudinal ionic current along the z-axis for a total of 20 simulations in system 2 provide noisy signals with high fluctuation frequency (Figure S1). The average translocation time (ns/nt) of five sets of simulations for each homo-oligonucleotide in system 2 showed the same trend, G > A > T > C, as in system 3 under 0.5 V longitudinal voltage bias in the presence of an electric field with a voltage bias of 4 and 10 V (Figures S3f and S5c). This order corresponds to the order of nucleotide size. However, Figures 4f and 4g demonstrate that the order of average transverse ionic current is G > C > A > T, and that of the average longitudinal ionic current is T > C > A > G. The order of the ionic currents does not correlate with the size of the nucleotides. Presumably, differences in orientation and conformation of the nucleotides are playing a role in modulation of ionic currents as simulations show nucleotides orientation and conformation vary for different homo-oligonucleotides during simulations.

The translocation times for A, T, G, and C homo-oligonucleotides in Figure 4 as well as Figures S3 and S5 vary slightly. G has longest translocation time, and C has the shortest one. However, it is noticeable that A and T, A and G, and T and C have similar values in Figure 4, Figure S3, and Figure S5, respectively. Purines A and G have two heterocyclic rings while pyrimidines T and C have only one single heterocyclic ring. The similarities between structures of A and G, T and C can explain the similarities of translocation times between A and G in Figure S3 and between T and C in Figure S5. However, the structures of A and G are not similar, which implies there are other factors involved in determination of the translocation time such as orientation and conformation of the nucleotides.

The average ionic currents order for different homo-oligonucleotide is not the same in system 2 (Figure 4f,g) and system 3 (Figures S3 and S5). The variation in volume of the pores and applied voltages from system 2 to system 3 can be one of the reasons of differences in the ionic currents order. In these simulations, for system 2, the highest difference in transverse ionic current was 30.73 pA between G and T, and the lowest difference was 0.36 pA between A and C homo-oligonucleotides. Correspondingly, these values in longitudinal
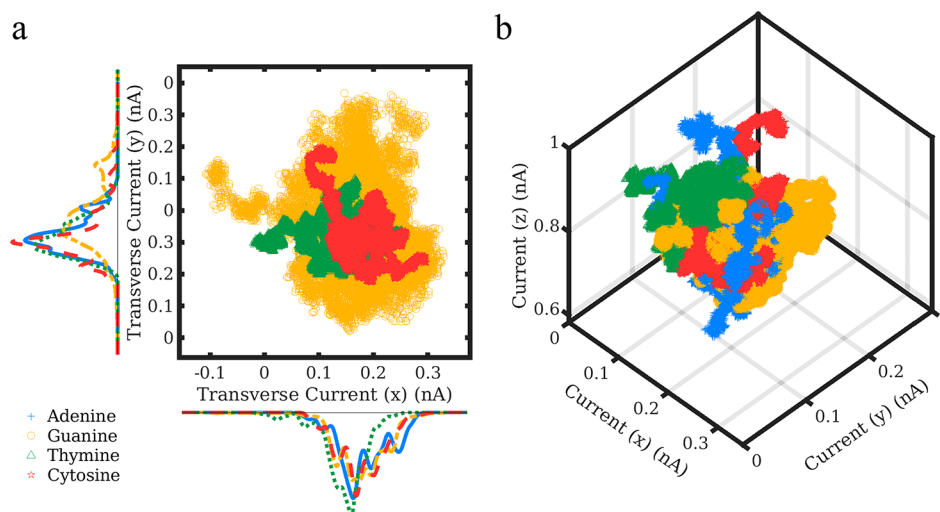
Figure 5. System 2: combination of transverse and longitudinal ionic currents. (a) A scatter plot of transverse ionic current (nA) in the *y* direction and transverse ionic current (nA) in the *x* direction. The Kernel fitted histogram of each ionic current is also represented individually on each axis. (b) A three-dimensional scatter plot of two transverse currents in the *x* and *y* directions and one longitudinal ionic current in the *z* direction. The axes are the averaged ionic currents generated through transverse nanochannels and longitudinal nanopore in system 2, which are presented in Figure 4a,d. *x* and *y* are directions of two transverse currents, and *z* is the direction of one longitudinal current.

ionic currents are 177.17 pA between T and G and 44.18 pA for T and C homo-oligonucleotides.

The small differences in the averaged ionic currents detected through the two transverse nanochannels were enhanced by combining the findings in 2D scatter plots. The scatter plot of two transverse ionic currents (nA) in Figure 5a shows that the ability to distinguish between homo-oligonucleotides is enhanced compared with the Kernel probability distribution of individual transverse ionic currents along the *x* and *y* directions through nanochannels, plotted along the axes of the 2D scatter plot. The adenine signal is hidden completely behind the signals of the other three oligonucleotides in the scatter plot, and the Kernel probability distributions of each type overlap broadly with each other. The cross-correlation of two transverse currents with longitudinal ionic current in Figures S2a−c indicates partial differentiation among four homo-oligonucleotides. Combining the signals detected through longitudinal nanopores with 2D scatter plots of two transverse ionic currents significantly enhances the ability to distinguish between the averaged signals, as indicated by the different colors in the 3D scatter plot of Figure 5b.

The instantaneous ionic currents are recorded every 10^{-12} s in which the small displacements of ions resulted from random thermal fluctuation is captured. The fluctuations of ions caused by thermal energy generate negative and positive ionic currents. However, force applied on ions from electric field leads to creation of a positive current on average. This is apparent in Figure 5 where we see mostly positive values for currents after we used a moving average over a 5 ns window of instantaneous ionic currents (Figure S1).

In our model, the voltage-driven ions that are traversing through the nanopores and nanochannels can enter through a nanopore and exit from a nanochannel, or vice versa, as there are two external fields perpendicular to each other. In view of this, we calculated the cross-correlation of two perpendicular currents in the longitudinal and transverse directions (Figures S2a−c). The cross-correlation of smoothed signals over a window of 1 ns demonstrates an enhanced ability to

distinguish the homo-oligonucleotides compared with using individual signals.

We applied a neural network (NN)—a supervised machine learning algorithm described in the Computational Methods section—to classify the ionic currents for each homo-oligonucleotide generated from three detectors perpendicular to each other (two transverse nanochannels and one longitudinal nanopore). The NN was unable to find a pattern in the ionic current signals; therefore, we used averaged signals to classify the four types of homo-oligonucleotides. We tested different sets of features extracted from the signals as NN inputs to obtain high classification accuracy. Among the tested features in the time and frequency domains, the averaged ionic current in the time domain contained significant information. The NN showed classification accuracy of around 50% by using signals from individual detectors. The accuracy exceeded 60% when we selected features obtained from different combinations of two detectors. The training and testing classification accuracy (Figure 6a,b) exceeded 80% when we used features from three detectors measuring the currents generated across the Si_3N_4 nanopore and nanochannels with different orientations of homo-oligonucleotides.

The ion−nucleotide interaction signals that contribute to ionic current generation were hidden in the random noise that resulted from thermal fluctuations of the ions in the simulations with the high sampling frequency. Although the NN was able to classify the averaged ionic currents with an accuracy of over 80%, this does not imply that the signal-to-noise ratio (SNR) for the averaged ionic currents increased. The substantial increase in classification accuracy may simply be a result of the similarity of the averaged random thermal fluctuations during the different simulations.

As previously discussed, one of the challenges in distinguishing between the nucleotides of ssDNA in time series signals is separating the effect of the neighboring and slightly dissimilar nucleotides in the generated signal. Consequently, to remove the neighbor effect for the sake of simplicity, we used homo-oligonucleotide ssDNA in the system simulations. The signal modulation caused by homo-oligonucleotides was determined

a

b
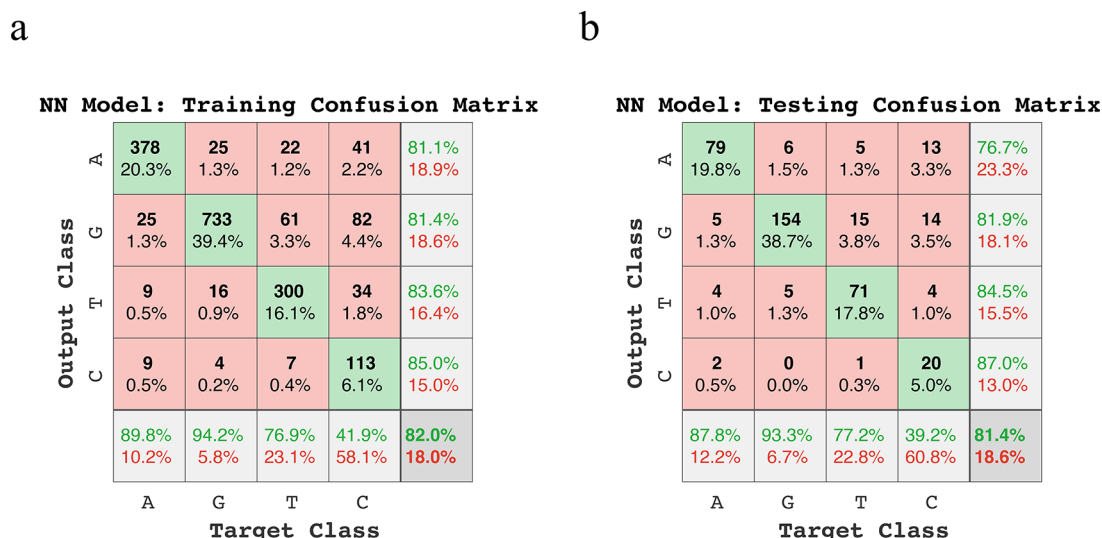
Figure 6. System 2: confusion matrix for NN classification. (a) Training accuracy of the NN in the classification of homo-oligonucleotide types. (b) Testing accuracy of the trained NN for classification of homo-oligonucleotide types. Green percentages represent the classification accuracies percentages, and red percentages represent the classification errors percentages.

for each nucleotide type A, G, T, and C. Note that the first and last nucleotides of a ssDNA have only one neighbor while others have two neighbors. Therefore, we analyzed the signals when the pore was fully occupied with the homo-oligonucleotides. In addition, this gives an approximately equal number of atoms blocking the ionic current during the collection of the signals.

The purpose of developing this model and performing molecular dynamics (MD) simulations was to distinguish between nucleotides by calculating the transverse and longitudinal ionic current modulation caused by nucleotides inside the nanopore. In the nanopore DNA sequencing method, deciphering the four nucleotide types depends on the information generated by the potential differences between ion–nucleotide interactions within nanopores. Under applied voltages, our simulations indicate slight differences in the ionic current signals of nucleotides—in the range of picoamperes—which, in applied experiment regimes would require high-resolution instrumentation to differentiate. Calculations made using the idealized MD model give noisy signals that only provide a small amount of information, which make it difficult to reach meaningful conclusions. The major drawback of the idealized MD model is the fast translocation of ssDNA, which results in insufficient time for ions to interact with each nucleotide at our studied voltage bias.

Irrespective of the sampling frequency limitation for experimental studies due to amplifier bandwidth, even for theoretical studies 1 nt/ns is considered a high translocation rate as there are not many ions interacting with each nucleotide traversing through the pore in a 1 THz ionic current sampling frequency to allow the nucleotides to be distinguished. Interaction between ions and single nucleotides is crucial in nanopore DNA sequencing using an ionic current, irrespective of the number of measured signals. The ionic current signals for the detection of the four nucleotide types are dependent on the differences in the ion–nucleotide interaction forces. Slow translocation provides sufficient time for ion–nucleotide interactions, which in turn can increase the SNR for single nucleotide detection. However, because of the simulation cost and the need to achieve meaningful statistical

analysis on an adequate number of signals within a given time period, we did not reduce the applied voltage bias below 0.5 V in our nanopore DNA sequencing simulations.

◼ CONCLUSIONS

This work studied the stepwise translocation of ssDNA in 1 M KCl solutions through a solid-state silicon nitride nanopore. The ionic currents are generated under an applied voltage bias along the pore in the presence of a transversely applied voltages through nanochannels perpendicular to the pore. Using this precisely engineered MD model, we anticipated homo-oligonucleotides are distinguishable because of the informative ion–nucleotide interactions by measuring the ionic current of K^+ and Cl^- ions through nanopore and nanochannels. However, the randomness of instantaneous ionic currents implied that the signals were hidden in random thermal fluctuations of ionic currents, and they were difficult to extract. We showed the averaged ionic currents for different types of homo-oligonucleotides were partially distinguishable. The combination of three averaged signals measured simultaneously through two transverse nanochannels and one longitudinal nanopore resulted in an enhanced ability to distinguish between homo-oligonucleotides. These findings suggest that the potential information in transverse and longitudinal signals can be an indicator of nucleotide types in robust and precisely engineered solid-state nanopores. The classification accuracy of the signals suggests that adding more indicators to the system could conceivably enhance its prediction power for the classification of nucleotides. The translocation rate of homo-oligonucleotides through the nanopore could be used as another predictive feature in addition to the ionic current. Furthermore, sequencing ssDNA by using ionic current requires a large data set and lower voltages with slow translocation of sequences through the nanopores to enable nucleotide discrimination, both of which would require greater computational resources for MD simulation.[68] This enhances the SNR as the available time for ion–nucleotide interactions increases. Finally, because of the small size of their interacting particles, i.e., electrons or

photons, spectroscopy and microscopy techniques could revolutionize the nanopore DNA sequencing method.

ASSOCIATED CONTENT

Ⓢ Supporting Information

The Supporting Information is available free of charge at https://pubs.acs.org/doi/10.1021/acsanm.9b02280.

> System 2: we include additional analysis on the same data obtained from MD simulations; system 3: we include calculations of the transverse and longitudinal ionic currents through a thin Si_3N_4 nanosheet; we performed simulations with two different transverse voltage of 4 and 10 V; we present a schematic of the system 3; we illustrate similar calculations to system 2 including individual average currents, individual Kernel distribution of longitudinal and transverse ionic currents, 2D ionic currents, and cross-correlation of longitudinal and transverse ionic currents (PDF)

AUTHOR INFORMATION

Corresponding Author

Jayendran C. Rasaiah − *University of Maine, Orono, Maine;* ⓘ orcid.org/0000-0002-4453-7438; Email: rasaiah@maine.edu

Other Author

Mohsen Farshad − *University of Maine, Orono, Maine;* ⓘ orcid.org/0000-0001-5095-4361

Complete contact information is available at:
https://pubs.acs.org/10.1021/acsanm.9b02280

Notes

The authors declare no competing financial interest.

REFERENCES

(1) Bezrukov, S.; Vodyanoy, I.; Parsegian, V. Counting Polymers Moving Through a Single Ion Channel. *Nature* **1994**, *370*, 279−281.

(2) Church, G.; Deamer, D. W.; Branton, D.; Baldarelli, R.; Kasianowicz, J. Characterization of Individual Polymer Molecules Based On Monomer interface-Interactions. US Patent 5,795,782, 1995.

(3) Kasianowicz, J.; Brandin, E.; Branton, D.; Deamer, D. Characterization of Individual Polynucleotide Molecules Using a Membrane Channel. *Proc. Natl. Acad. Sci. U. S. A.* **1996**, *93*, 13770−13773.

(4) Song, L.; Hobaugh, M.; Shustak, C.; Cheley, S.; Bayley, H.; Gouaux, J. Structure of Staphylococcal Alpha-Hemolysin, a Heptameric Transmembrane Pore. *Science* **1996**, *274*, 1859−1865.

(5) Robertson, J. W. F.; Rodrigues, C. G.; Stanford, V. M.; Rubinson, K. A.; Krasilnikov, O. V.; Kasianowicz, J. J. Single-Molecule Mass Spectrometry in Solution Using a Solitary Nanopore. *Proc. Natl. Acad. Sci. U. S. A.* **2007**, *104*, 8207−8211.

(6) Reiner, J. E.; Kasianowicz, J. J.; Nablo, B. J.; Robertson, J. W. F. Theory for Polymer Analysis Using Nanopore-Based Single-Molecule Mass Spectrometry. *Proc. Natl. Acad. Sci. U. S. A.* **2010**, *107*, 12080−12085.

(7) Balijepalli, A.; Ettedgui, J.; Cornio, A. T.; Robertson, J. W. F.; Cheung, K. P.; Kasianowicz, J. J.; Vaz, C. Quantifying Short-Lived Events in Multistate Ionic Current Measurements. *ACS Nano* **2014**, *8*, 1547−1553.

(8) Akeson, M.; Branton, D.; Kasianowicz, J.; Brandin, E.; Deamer, D. Microsecond Time-Scale Discrimination Among Polycytidylic Acid, Polyadenylic Acid, and Polyuridylic Acid as Homopolymers or as Segments Within Single RNA Molecules. *Biophys. J.* **1999**, *77*, 3227−3233.

(9) Meller, A.; Nivon, L.; Brandin, E.; Golovchenko, J.; Branton, D. Rapid Nanopore Discrimination Between Single Polynucleotide Molecules. *Proc. Natl. Acad. Sci. U. S. A.* **2000**, *97*, 1079−1084.

(10) Meller, A.; Nivon, L.; Branton, D. Voltage-Driven DNA Translocations Through a Nanopore. *Phys. Rev. Lett.* **2001**, *86*, 3435−3438.

(11) Ashkenasy, N.; Sánchez-Quesada, J.; Bayley, H.; Ghadiri, M. Recognizing a Single Base in an Individual DNA Strand: A Step Toward DNA Sequencing in Nanopores. *Angew. Chem.* **2005**, *117*, 1425−1428.

(12) Lagerqvist, J.; Zwolak, M.; Di Ventra, M. Fast DNA Sequencing via Transverse Electronic Transport. *Nano Lett.* **2006**, *6*, 779−782.

(13) Zwolak, M.; Di Ventra, M. Electronic Signature of DNA Nucleotides via Transverse Transport. *Nano Lett.* **2005**, *5*, 421−424.

(14) Heng, J.; Aksimentiev, A.; Ho, C.; Dimitrov, V.; Sorsch, T.; Miner, J.; Mansfield, W.; Schulten, K.; Timp, G. Beyond the Gene Chip. *Bell Syst. Technol. J.* **2005**, *10*, 5−22.

(15) Gracheva, M.; Xiong, A.; Aksimentiev, A.; Schulten, K.; Timp, G.; Leburton, J. Simulation Of The Electric Response of DNA Translocation Through a Semiconductor Nanopore-Capacitor. *Nanotechnology* **2006**, *17*, 622−633.

(16) Sigalov, G.; Comer, J.; Timp, G.; Aksimentiev, A. Detection of DNA Sequences Using an Alternating Electric Field in a Nanopore Capacitor. *Nano Lett.* **2008**, *8*, 56−63.

(17) Soni, G.; Meller, A. Progress Toward Ultrafast DNA Sequencing Using Solid-State Nanopores. *Clin. Chem.* **2007**, *53*, 1996−2001.

(18) Anderson, B. N.; Assad, O. N.; Gilboa, T.; Squires, A. H.; Bar, D.; Meller, A. Probing Solid-State Nanopores with Light for the Detection of Unlabeled Analytes. *ACS Nano* **2014**, *8*, 11836−11845.

(19) Wang, R.; Gilboa, T.; Song, J.; Huttner, D.; Grinstaff, M.; Meller, A. Single-Molecule Discrimination Of Labeled DNAs And Polypeptides Using Photoluminescent-Free TiO_2 Nanopores. *ACS Nano* **2018**, *12*, 11648−11656.

(20) Feng, Y.; Zhang, Y.; Ying, C.; Wang, D.; Du, C. Nanopore-Based Fourth-Generation DNA Sequencing Technology. *Genomics, Proteomics Bioinf.* **2015**, *13*, 4−16.

(21) Wang, Y.; Yang, Q.; Wang, Z. The Evolution of Nanopore Sequencing. *Front. Genet.* **2015**, *5*, 449.

(22) Jain, M.; Olsen, H.; Paten, B.; Akeson, M. The Oxford Nanopore Minion: Delivery of Nanopore Sequencing to the Genomics Community. *Genome Biol.* **2016**, *17*, 239.

(23) Zwolak, M.; Di Ventra, M. Colloquium: Physical Approaches To DNA Sequencing And Detection. *Rev. Mod. Phys.* **2008**, *80*, 141−165.

(24) Butler, T.; Pavlenok, M.; Derrington, I.; Niederweis, M.; Gundlach, J. Single-Molecule DNA Detection with an Engineered MspA Protein Nanopore. *Proc. Natl. Acad. Sci. U. S. A.* **2008**, *105*, 20647−20652.

(25) Derrington, I.; Butler, T.; Collins, M.; Manrao, E.; Pavlenok, M.; Niederweis, M.; Gundlach, J. Nanopore DNA Sequencing with MspA. *Proc. Natl. Acad. Sci. U. S. A.* **2010**, *107*, 16060−16065.

(26) Manrao, E.; Derrington, I.; Pavlenok, M.; Niederweis, M.; Gundlach, J. Nucleotide Discrimination with DNA Immobilized in the MspA Nanopore. *PLoS One* **2011**, *6*, No. e25723.

(27) Manrao, E.; Derrington, I.; Laszlo, A.; Langford, K.; Hopper, M.; Gillgren, N.; Pavlenok, M.; Niederweis, M.; Gundlach, J. Reading

DNA at Single-Nucleotide Resolution with a Mutant Mspa Nanopore and Phi29 DNA Polymerase. *Nat. Biotechnol.* **2012**, *30*, 349−353.

(28) Garalde, D. R.; Snell, E. A.; Jachimowicz, D.; Sipos, B.; Lloyd, J. H.; Bruce, M.; Pantic, N.; Admassu, T.; James, P.; Warland, A.; Jordan, M.; Ciccone, J.; Serra, S.; Keenan, J.; Martin, S.; McNeill, L.; Wallace, E. J.; Jayasinghe, L.; Wright, C.; Blasco, J.; et al. Highly Parallel Direct RNA Sequencing on an Array of Nanopores. *Nat. Methods* **2018**, *15*, 201−206.

(29) Jain, M.; Koren, S.; Miga, K. H.; Quick, J.; Rand, A. C.; Sasani, T. A.; Tyson, J. R.; Beggs, A. D.; Dilthey, A. T.; Fiddes, I. T.; Malla, S.; Marriott, H.; Nieto, T.; O'Grady, J.; Olsen, H. E.; Pedersen, B. S.; Rhie, A.; Richardson, H.; Quinlan, A. R.; Snutch, T. P.; et al. Nanopore Sequencing And Assembly Of A Human Genome With Ultra-Long Reads. *Nat. Biotechnol.* **2018**, *36*, 338−345.

(30) Majd, S.; Yusko, E.; Billeh, Y.; Macrae, M.; Yang, J.; Mayer, M. Applications of Biological Pores in Nanomedicine, Sensing, and Nanoelectronics. *Curr. Opin. Biotechnol.* **2010**, *21*, 439−476.

(31) Venkatesan, B.; Bashir, R. Nanopore Sensors for Nucleic Acid Analysis. *Nat. Nanotechnol.* **2011**, *6*, 615−624.

(32) Branton, D.; Deamer, D. W. *NANOPORE SEQUENCING: An Introduction*; World Scientific Publishing Co. Pte. Ltd.: 2019.

(33) Liu, Z.; Wang, Y.; Deng, T.; Chen, Q. Solid-State Nanopore-Based DNA Sequencing Technology. *J. Nanomater.* **2016**, *2016*, 1−13.

(34) Fologea, D.; Gershow, M.; Ledden, B.; McNabb, D.; Golovchenko, J.; Li, J. Detecting Single Stranded DNA with a Solid State Nanopore. *Nano Lett.* **2005**, *5*, 1905−1909.

(35) Dekker, C. Solid-State Nanopores. *Nat. Nanotechnol.* **2007**, *2*, 209−215.

(36) Storm, A.; Chen, J.; Ling, X.; Zandbergen, H.; Dekker, C. Fabrication of Solid-State Nanopores with Single-Nanometre Precision. *Nat. Mater.* **2003**, *2*, 537−540.

(37) Heng, J.; Ho, C.; Kim, T.; Timp, R.; Aksimentiev, A.; Grinkova, Y.; Sligar, S.; Schulten, K.; Timp, G. Sizing DNA Using a Nanometer-Diameter Pore. *Biophys. J.* **2004**, *87*, 2905−2911.

(38) Venkatesan, B.; Dorvel, B.; Yemenicioglu, S.; Watkins, N.; Petrov, I.; Bashir, R. Highly Sensitive, Mechanically Stable Nanopore Sensors for DNA Analysis. *Adv. Mater.* **2009**, *21*, 2771−2776.

(39) van den Hout, M.; Krudde, V.; Janssen, X.; Dekker, N. Distinguishable Populations Report on the Interactions of Single DNA Molecules with Solid-State Nanopores. *Biophys. J.* **2010**, *99*, 3840−3848.

(40) Nam, S.; Rooks, M.; Kim, K.; Rossnagel, S. Ionic Field Effect Transistors With Sub-10 nm Multiple Nanopores. *Nano Lett.* **2009**, *9*, 2044−2048.

(41) McNally, B.; Singer, A.; Yu, Z.; Sun, Y.; Weng, Z.; Meller, A. Optical Recognition of Converted DNA Nucleotides for Single-Molecule DNA Sequencing Using Nanopore Arrays. *Nano Lett.* **2010**, *10*, 2237−2244.

(42) Li, J.; Stein, D.; McMullan, C.; Branton, D.; Aziz, M.; Golovchenko, J. Ion-Beam Sculpting at Nanometre Length Scales. *Nature* **2001**, *412*, 166−169.

(43) Li, J.; Gershow, M.; Stein, D.; Brandin, E.; Golovchenko, J. DNA Molecules and Configurations in a Solid-State Nanopore Microscope. *Nat. Mater.* **2003**, *2*, 611−615.

(44) Aksimentiev, A.; Heng, J.; Timp, G.; Schulten, K. Microscopic Kinetics of DNA Translocation Through Synthetic Nanopores. *Biophys. J.* **2004**, *87*, 2086−2097.

(45) Gumbart, J.; Wang, Y.; Aksimentiev, A.; Tajkhorshid, E.; Schulten, K. Molecular Dynamics Simulations of Proteins in Lipid Bilayers. *Curr. Opin. Struct. Biol.* **2005**, *15*, 423−431.

(46) Aksimentiev, A. Deciphering Ionic Current Signatures of DNA Transport Through a Nanopore. *Nanoscale* **2010**, *2*, 468−483.

(47) Wilson, J.; Di Ventra, M. Single-Base DNA Discrimination via Transverse Ionic Transport. *Nanotechnology* **2013**, *24*, 415101.

(48) Boynton, P.; Di Ventra, M. Sequencing Proteins with Transverse Ionic Transport in Nanochannels. *Sci. Rep.* **2016**, *6*, 25232.

(49) van Dijk, M.; Bonvin, A. 3D-DART: A DNA Structure Modelling Server. *Nucleic Acids Res.* **2009**, *37*, W235−W239.

(50) Humphrey, W.; Dalke, A.; Schulten, K. VMD: Visual Molecular Dynamics. *J. Mol. Graphics* **1996**, *14*, 33−38.

(51) Phillips, J.; Braun, R.; Wang, W.; Gumbart, J.; Tajkhorshid, E.; Villa, E.; Chipot, C.; Skeel, R.; Kalé, L.; Schulten, K. Scalable Molecular Dynamics with NAMD. *J. Comput. Chem.* **2005**, *26*, 1781−1802.

(52) MacKerell, A. D.; Bashford, D.; Bellott, M.; Dunbrack, R. L.; Evanseck, J. D.; Field, M. J.; Fischer, S.; Gao, J.; Guo, H.; Ha, S.; Joseph-McCarthy, D.; Kuchnir, L.; Kuczera, K.; Lau, F. T. K.; Mattos, C.; Michnick, S.; Ngo, T.; Nguyen, D. T.; Prodhom, B.; Reiher, W. E.; et al. All-Atom Empirical Potential for Molecular Modeling and Dynamics Studies of Proteins. *J. Phys. Chem. B* **1998**, *102*, 3586−3616.

(53) Darden, T.; York, D.; Pedersen, L. Particle Mesh Ewald: An N·Log(N) Method for Ewald Sums in Large Systems. *J. Chem. Phys.* **1993**, *98*, 10089−10092.

(54) Qiu, H.; Sarathy, A.; Leburton, J.; Schulten, K. Intrinsic Stepwise Translocation of Stretched ssDNA in Graphene Nanopores. *Nano Lett.* **2015**, *15*, 8322−8330.

(55) Luan, B.; Stolovitzky, G.; Peng, H.; Harrer, S.; Waggoner, P.; Polonsky, S.; Rossnagel, S.; Martyna, G. Characterizing and Controlling the Motion of ssDNA in a Solid-State Nanopore. *Biophys. J.* **2011**, *100*, 2214−2222.

(56) Wells, D.; Belkin, M.; Comer, J.; Aksimentiev, A. Assessing Graphene Nanopores for Sequencing DNA. *Nano Lett.* **2012**, *12*, 4117−4123.

(57) Craig, J.; Laszlo, A.; Brinkerhoff, H.; Derrington, I.; Noakes, M.; Nova, I.; Tickman, B.; Doering, K.; de Leeuw, N.; Gundlach, J. Revealing Dynamics of Helicase Translocation on Single-Stranded DNA Using High-Resolution Nanopore Tweezers. *Proc. Natl. Acad. Sci. U. S. A.* **2017**, *114*, 11932−11937.

(58) Luan, B.; Zhou, R. Spontaneous Transport of Single-Stranded DNA Through Graphene−Mos2 Heterostructure Nanopores. *ACS Nano* **2018**, *12*, 3886−3891.

(59) Storm, A.; Storm, C.; Chen, J.; Zandbergen, H.; Joanny, J.; Dekker, C. Fast DNA Translocation Through a Solid-State Nanopore. *Nano Lett.* **2005**, *5*, 1193−1197.

(60) Luan, B.; Stolovitzky, G.; Martyna, G. Slowing and Controlling the Translocation of DNA in a Solid-State Nanopore. *Nanoscale* **2012**, *4*, 1068−1077.

(61) Wanunu, M.; Sutin, J.; McNally, B.; Chow, A.; Meller, A. DNA Translocation Governed by Interactions with Solid-State Nanopores. *Biophys. J.* **2008**, *95*, 4716−4725.

(62) Ramachandran, A.; Liu, Y.; Asghar, W.; Iqbal, S. Character-ization of DNA-Nanopore Interactions by Molecular Dynamics. *Am. J. Biomed. Sci.* **2009**, 344−351.

(63) Timp, W.; Mirsaidov, U.; Wang, D.; Comer, J.; Aksimentiev, A.; Timp, G. Nanopore Sequencing: Electrical Measurements of the Code of Life. *IEEE Trans. Nanotechnol.* **2010**, *9*, 281−294.

(64) Maitra, R.; Kim, J.; Dunbar, W. Recent Advances in Nanopore Sequencing. *Electrophoresis* **2012**, *33*, 3418−3428.

(65) Venta, K.; Shemer, G.; Puster, M.; Rodríguez-Manzo, J.; Balan, A.; Rosenstein, J.; Shepard, K.; Drndić, M. Differentiation of Short, Single-Stranded DNA Homopolymers in Solid-State Nanopores. *ACS Nano* **2013**, *7*, 4629−4636.

(66) Balan, A.; Machielse, B.; Niedzwiecki, D.; Lin, J.; Ong, P.; Engelke, R.; Shepard, K.; Drndić, M. Improving Signal-To-Noise Performance for DNA Translocation in Solid-State Nanopores at MHz Bandwidths. *Nano Lett.* **2014**, *14*, 7215−7220.

(67) Meller, A.; Branton, D. Single Molecule Measurements of DNA Transport Through a Nanopore. *Electrophoresis* **2002**, *23*, 2583−2591.

(68) Editorial. The Long View on Sequencing. *Nat. Biotechnol.* **2018**, *36* (4), 287−287.